Supplementary materials

Thermal stability and hcp-fcc allotropic transformation in supported Co metal catalysts probed *near operando* by ferromagnetic NMR

Andrey S. Andreev[a,b,c], Jean-Baptiste d'Espinose de Lacaillerie*[,c], Olga B. Lapina[a,b], Alexander Gerashenko[d]

[a] Pirogova str. 2, Novosibirsk State University (NSU), Novosibirsk, 630090, Russia

[b] Pr. Lavrentieva 5, Solid-State NMR group, Boreskov Institute of Catalysis SB RAS (BIC SB RAS), Novosibirsk, 630090, Russia

[c] 10 Rue Vauquelin, Soft Matter Sciences and Engineering (SIMM), UMR CNRS 7615, PSL Research University, ESPCI ParisTech, Paris, 75005, France

[d] S. Kovalevskoy str. 18, Kinetic Phenomena laboratory, Institute of Metals Physics UB RAS, Ekaterinburg, 620041, Russia

The ferromagnetic NMR signal

The theory of magnetic resonance in magnetic materials, albeit complex, is well understood and has been described elsewhere with great clarity in books and reviews [1].Only relevant aspects are recalled here.

The total magnetization of the sample, M_T, results from the sum of two magnetizations, electronic (M) and nuclear (m):

$$\vec{M}_T = \vec{M} + \vec{m}.$$

Those two magnetizations are coupled through two Bloch equations

$$\frac{d\vec{m}}{dt} = \gamma_n \vec{m} \times \vec{b} + \vec{r}$$
$$\frac{d\vec{M}}{dt} = \gamma_e \vec{M} \times \vec{B} + \vec{R} \qquad (1S)$$

Where b (B), r (R), and γ_n (γ_e) are the magnetic field felt by the nucleus (electron), the relaxation of the nuclear (electronic) magnetization and gyromagnetic ratio of the nucleus (electron). In the absence of a permanent external field, within the molecular field approximation and identifying the magnetic hyperfine field felt by the nuclei with the molecular field, the local fields can be written as

$$\vec{b} = \vec{B}_1 e^{i\omega t} + \lambda_m \vec{M} = \vec{B}_1 e^{i\omega t} + \vec{B}_{hf}$$
$$\vec{B} = \vec{B}_a + \vec{B}_1 e^{i\omega t} + \lambda_m \vec{m}$$

where λ_m is the molecular field parameter.
Looking for the stationary solutions of equations (1S) leads to the determination of the ferromagnetic nuclear magnetic resonance (FNR) and the ferromagnetic electronic resonance frequency (FMR)

$$FNR: \Omega_n = \left| -\gamma_n \left[B_{hf} \left(1 - \eta_d \frac{m}{M} \right) \right] \right|$$
$$FMR: \Omega_e = \left| -\gamma_e \left[B_a \left(1 + \eta_d \frac{m}{M} \right) \right] \right| \quad (2S)$$

where $\eta_d = B_{hf}/B_a$, m and M are the amplitudes of the nuclear and electronic magnetization respectively. The frequency pulling associated with the second term of each resonance frequency has been discussed by de Gennes [2], but in metallic cobalt in the range of temperatures studied here, $m/M << 1$ and the frequencies can be approximated with a good level of confidence as simply

$$\Omega_n \approx \left| -\gamma_n B_{hf} \right| = \left| -\gamma_n \lambda_m M \right|$$
$$\Omega_e \approx \left| -\gamma_e B_a \right| \quad (3S)$$

As far as the ferromagnetic NMR frequency is concerned, in the bulk, it is thus simply the Larmor frequency in the hyperfine field proportional to the electronic magnetization. In small particles with a limited number of domains (mainly single-domain particles), the demagnetization field must be added (note that the hyperfine field is negative in Co metal). Because we operated near the nuclear resonance frequency and since the experimental setup was a conventional NMR one (detection by Faraday induction in a solenoid), the signal was directly proportional to the total nuclear transverse magnetization [3]. In a sample containing several crystallites and magnetic domains, integration must be performed over all the relative orientations of the RF field with respect to of the hyperfine field. Building on [4], the transverse magnetization echo intensity after two-pulse at resonance with the nuclei and of equal duration τ has been derived [5] leading to the following expression for the signal from the ferromagnetic domains

$$E_T^d \propto \frac{V_d}{V_d + V_w} \frac{\eta_d m}{\alpha^2} \left[\sin\alpha - \frac{1}{8}\sin 2\alpha - \alpha\cos\alpha + \frac{1}{4}\alpha\cos 2\alpha \right] G\left(\Delta / T_2^* \right) \quad (4S)$$
$$\alpha = \gamma_n \eta_d B_1 \tau$$

where V_d and V_w are the volumes of domains and walls respectively. The function $G(\Delta/T_2^*)$ accounts for the decay Δ during the interpulse with a characteristic time T_2^* (Fourier transform of the lineshape).
For the domain walls, the situation is more complex. The spatial variation of the hyperfine and anisotropy fields within the walls, and the motion of the walls under the influence of the rf field must be taken into account. Furthermore, assumptions on the particle size (D), wall structures, and distributions must be made[4]. In any case, the following behaviour can be expected for the part of the echo arising from the nuclei within the domain walls

$$E_T^w \propto \frac{V_w}{V_d + V_w} \eta_{0w}\, m\, F\left(\alpha_0, \eta_{0w}, D, \ldots\right) G\left(\Delta / T_2^* \right)$$
$$\eta_{0w} = a\eta_d \quad (5S)$$
$$\alpha_0 = \gamma_n \eta_{0w} B_1 \tau$$

Where the proportionality factor $a > 1$ between the domain enhancement factor and the maximum enhancement factor accounts for the angle between the magnetic moments of adjacent atoms [4,6]. The function F will depend on the way the walls are modelled. Concerning the temperature behaviour of the ferromagnetic signal, from the above equations, the following conclusion can be drawn. The resonance frequency Ω_n is expected to vary simply as the hyperfine field. In turn, the electronic magnetization M and hyperfine constant λ_m can have a more complex temperature dependence [7] . The temperature dependence of the echo intensity from the domains and domain walls is thus not expected to be straightforward according to (4S) and (5S). The nuclear equilibrium magnetization m is expected to vary as $1/T$ while the one of M is dictated by spin-waves theory [8].

TEM and XRD characterization

Experimental

The samples used fot characterization were not exposed to air. They were manipulated in a glove box under argon atmosphere and conserved in hexane for HRTEM study. Prior to TEM measurements a drop of the sample suspension in hexane with sample was put onto a copper grid and immediately transferred into the microscope chamber. By capillarity, hexane remains inside the pores and the bulk of the sample is thus protected from air. TEM working by transmission, surface oxygen oxidation does not contribute significantly to the signal. For XRD measurements, the samples were evacuated under argon atmosphere and transferred into hermetically locking XRD probe.

HRTEM micrographs were obtained with a JEM-2010 microscope (JEOL Co) with a lattice resolution of 0.14 nm and an accelerating voltage of 200 kV. The high-resolution images of periodic structures were analyzed by the Fast Fourier transformation (FFT) method. Local energy-dispersive X-ray (EDX) analysis was carried out on an EDAX spectrometer (EDAX Co) fitted with a Si (Li) detector with a resolution of 130 eV. Samples to be examined by HRTEM were prepared on a holey carbon film mounted on a copper grid.

The X-ray diffraction (XRD) patterns were acquired using a X'TRA (Thermo ARL) diffractometer (Bragg–Brentano geometry, CuKa radiation, energy dispersed detector, step scan mode). Data acquisition was performed with a 2θ angle range from 30° to 80°, a step of 0.05° and an accumulation time of 9 s per point.

TEM

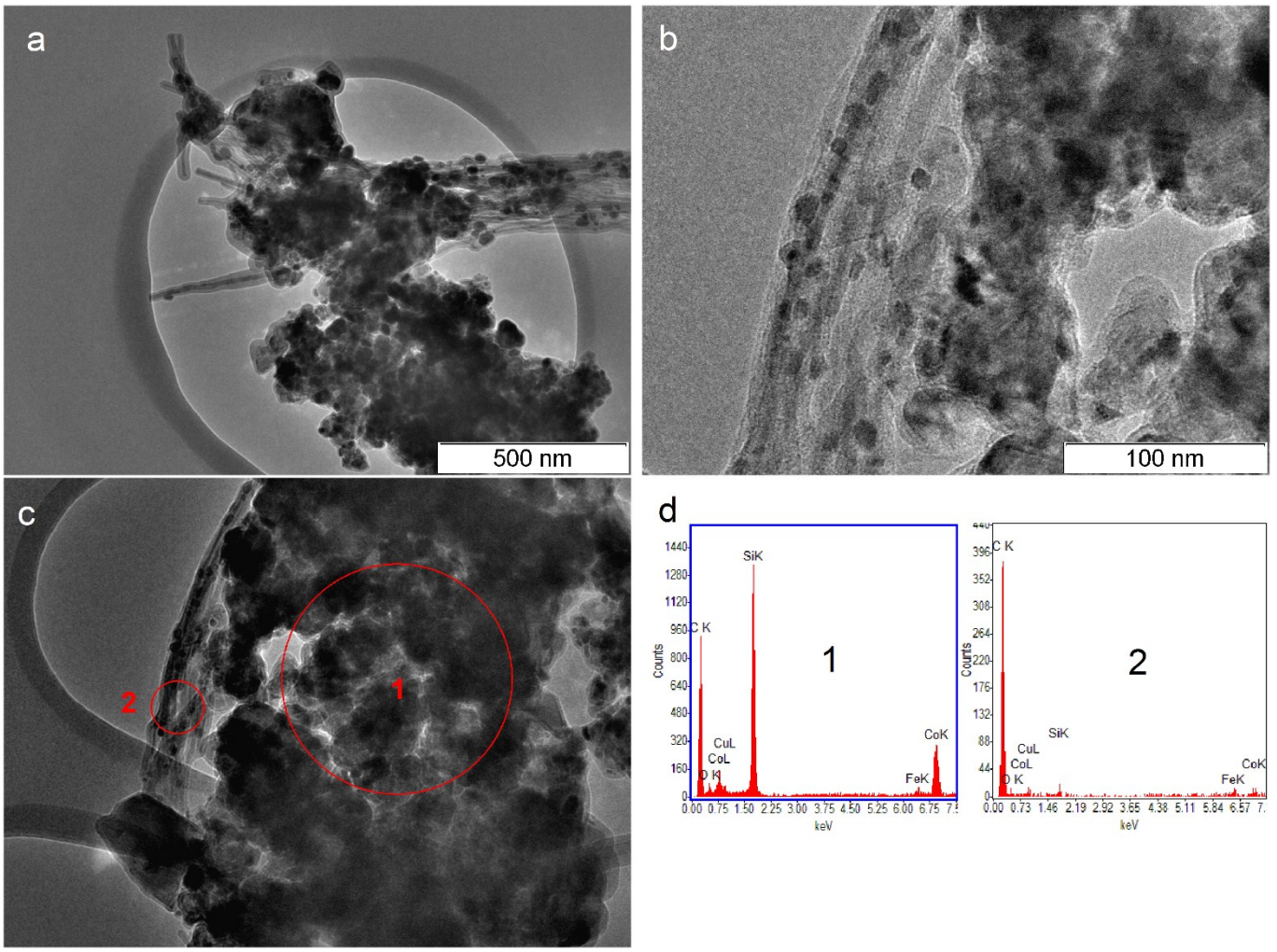

Fig. S1. HRTEM images of initial sample showing morphology and particle sizes (a) - (b); (c) – (d) HRTEM image of Co-Fig S1. HRTEM images of low resolution showing morphology of the sample and Co particle sizes (a)-(b); (c)-(d) HRTEM image of cobalt containng (1) and cobalt free (2) part of the initial sample. Hightened carbon content is a result of residual hexane content in the sample pores.

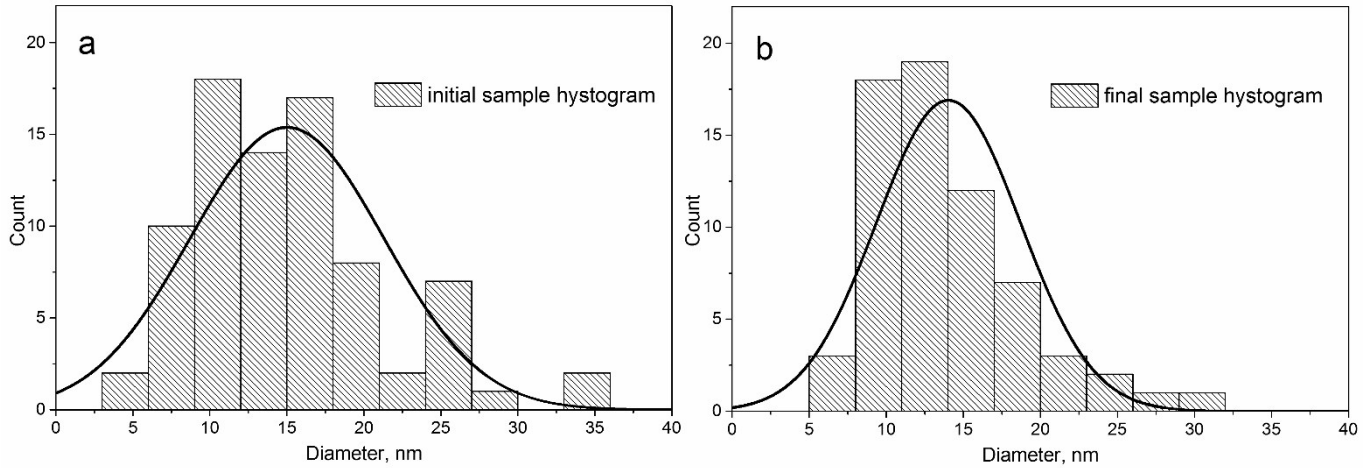

Fig. S2. A histogram obtained from HRTEM anakysis of the sample before (a) and after heating in the NMR spectrometer (b).

HRTEM images n Fig. S1 display the morphology and structure of Co/SiC catalysts. EDX images in Fig S1d show Co free and Co-containing parts of the sample. The histograms shown in Figure S2 state the conservation of average Co particle size after temperature experiment.

XRD

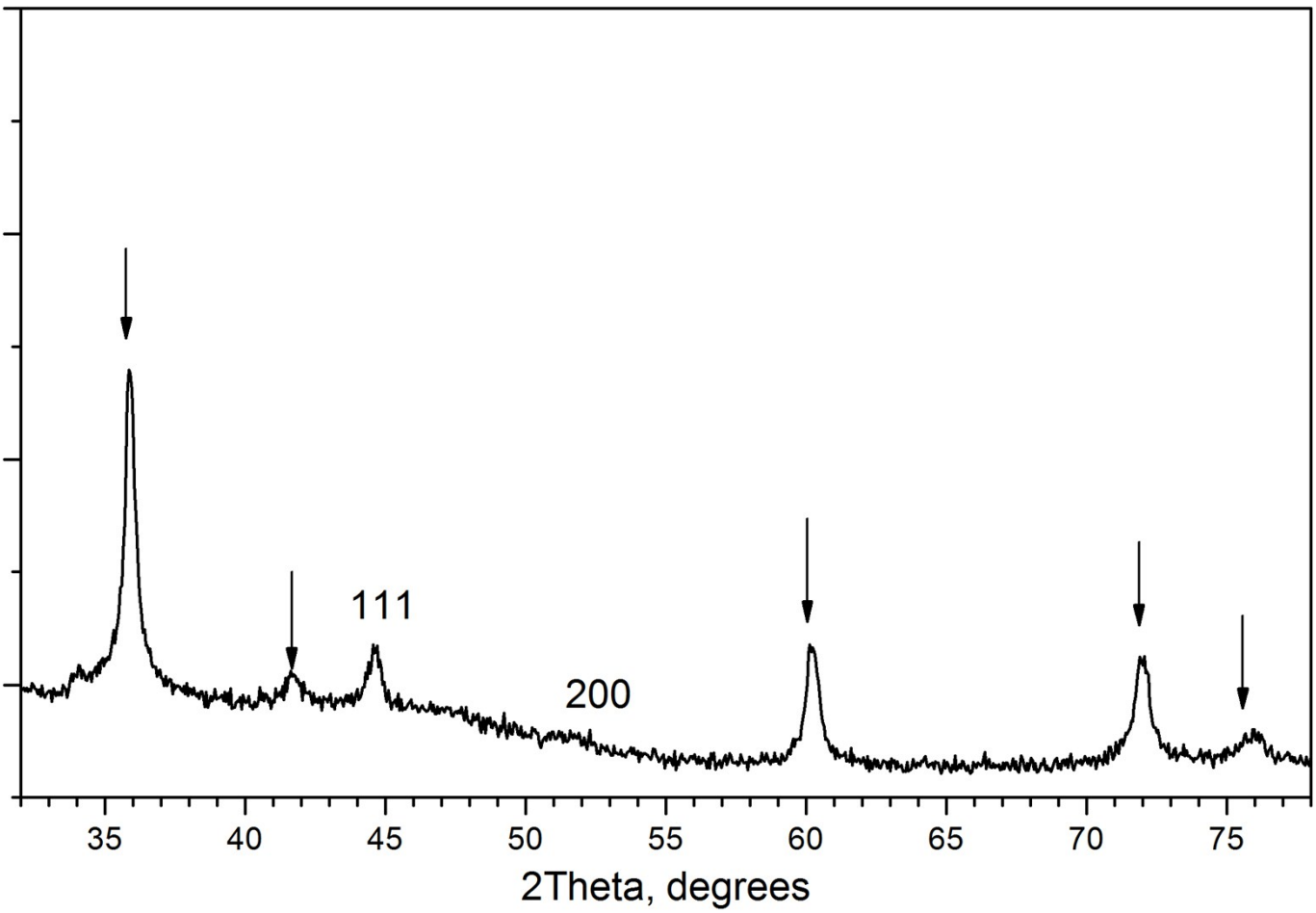

Fig. S3. XRD pattern of the initial reduced sample of Co/SiC. Arrows indicate SiC diffraction peaks (3C polytype, space group F4(-)3m). Numbers show fcc Co diffraction peaks.

The XRD pattern of the initial sample displays *111* fcc Co peaks in addition to the ones of SiC (shown by arrows). The *200* Co metal peak is highly broadened indicating a faulted structure for the fcc Co metal. It should be noticed that stacking faults (sf's) in hcp structure ABAB correspond to the ABC fcc structure. And conversely, sf's in fcc structure ABCABC correspond to layers of hcp structure. Therefore, the XRD observation of a highly faulted fcc structure is in a good agreement with ferromagnetic ^{59}Co NMR data, which evidenced the occurrence of both fcc and hcp stackings of Co metal.

References

1. A. P. Guimarães, *Magnetism and Magnetic Resonance in Solids*, John Wiley & Sons, Chichester, 1998.
2. P. G. de Gennes, P. A. Pincus, F. Hartmann-Boutron and J. M. Winter, *Phys. Rev.*, 1963, **129**, 1105–1115.
3. D. I. Hoult and N. S. Ginsberg, *J. Magn. Reson.*, 2001, **148**, 182–99.
4. M. Stearns, *Phys. Rev.*, 1967, **162**, 496–509.
5. I. S. Oliveira and A. P. Guimarães, *J. Magn. Magn. Mater.*, 1997, **170**, 277–284.
6. A. M. Portis and A. C. Gossard, *J. Appl. Phys.*, 1960, **31**, S205–S213.
7. D. M. Edwards, *J. Phys. F Met. Phys.*, 1976, **6**, L185–L189.
8. E. A. Turov and M. P. Petrov, *Nuclear Magnetic Resonance in Ferro- and Antiferromagnets*, Jerusalem : Israel Program for Scientific Tr. (Halsted Pr. N.Y.), 1972.